

## Original Article

# MicroRNA-21 released from mast cells-derived extracellular vesicles drives asthma in mice by potentiating airway inflammation and oxidative stress

Ying Zou, Qixing Zhou, Yunfeng Zhang

*Department of Respiratory and Critical Medicine, Shanghai Putuo District Liqun Hospital, Shanghai 200333, P. R. China*

Received March 4, 2021; Accepted April 29, 2021; Epub July 15, 2021; Published July 30, 2021

**Abstract:** Objective: Mast cells-derived extracellular vesicles (EVs) play vital roles in various physiological and pathophysiological conditions. However, the cargoes of mast cells-derived EVs in asthma have not been established. Here, we set to identify the role of microRNA-21 (miR-21) from mast cells-derived EVs in ozone- and lipopolysaccharide (LPS)-induced mouse airway epithelial cells (MIC-iCell-a006 cells) and asthmatic mice. Methods: After ozone or LPS treatment, MIC-iCell-a006 cells were subjected to a microarray analysis to screen differentially expressed miRNAs, and then co-cultured with EVs. miR-21 was silenced in cells, followed by CCK-8, scratch, and Transwell assays. Mice were challenged with ovalbumin, and antioxidant enzymes and inflammatory cell infiltration were assessed after EVs and miR-21 inhibitor treatments. The relation between miR-21 and DDAH1 was evaluated by Dual-Luciferase assay, and changes in Wnt/ $\beta$ -catenin pathway related proteins were examined by western blot. Finally, the involvement of the DDAH1/Wnt/ $\beta$ -catenin axis in miR-21-mediated oxidative stress and inflammation was verified by rescue experiments. Results: miR-21 expression was upregulated in MIC-iCell-a006 cells induced by ozone or LPS. miR-21 was enriched in mast cells-derived EVs, and EVs increased miR-21 expression in MIC-iCell-a006 cells. miR-21 inhibitor increased cell activity and alleviated oxidative stress and inflammation. In asthmatic mice, miR-21 expression was increased, and EVs decreased antioxidant enzymes and increased inflammatory cells, whose effects were reversed by miR-21 knockdown. miR-21 targeted DDAH1 to mediate the Wnt/ $\beta$ -catenin signaling, and down-regulation of DDAH1 inhibited the action of miR-21 inhibitor. Conclusion: The miR-21 secreted from mast cells-derived EVs promotes oxidative stress and inflammatory responses in asthmatic mice via the DDAH1/Wnt/ $\beta$ -catenin signaling axis.

**Keywords:** MicroRNA-21, DDAH1, Wnt/ $\beta$ -catenin pathway, oxidative stress, inflammatory responses

## Introduction

Airway epithelial cells locate at the boundary between the host and the environment and characterize the first line of the protection against microorganisms, gases, and allergens [1], which enable divergence from immune and inflammatory responses to external stimuli that are fundamental to the development of asthma [2]. Oxidative stress is a vital pathophysiological process of airway diseases such as asthma which leads to significant morbidity and mortality [3]. High level of ambient ozone has been suggested to contribute to the worsening of symptoms and increased hospitalization stays of patients with asthma, and exposure to ozone has been linked to airway inflam-

mation, oxidative stress, and bronchial hyper-responsiveness [4]. Therefore, more efforts should be focused on understanding the signaling pathways responsible for oxidative stress and airway inflammation to develop more targeted therapies for asthma.

Mast cells are well-known central effectors in IgE-mediated allergic diseases including asthma [5]. The mast cells that were discovered before allergy was identified as a regular immunological phenomenon are at the center of allergic inflammation, with IgE linking the connection between antigen (allergen) and the high-affinity IgE receptor on mast cells [6]. On top of that, mast cells also participate in a broad spectrum of cellular interactions during

disorders, for example, by delivering extracellular vesicles (EVs) [7]. Evidence has indicated that the contents and size distribution of EVs are highly heterogeneous, which depend on the cellular source, state and microenvironments, and three subgroups of EVs have been outlined: apoptotic bodies, microvesicles, and exosomes [8]. Mast cells-derived EVs have been demonstrated to show immuno-stimulative effects on B cells and T cells, highlighting their great significance in physiological and pathophysiological conditions [9, 10]. More specifically, EVs derived from mast cells involved in asthma have the potency to activate other asthma-related cells [11]. Mast cells share close vicinity to epithelial cells in the airways, and they can communicate with each other by delivering EVs which have great number of cargoes, including proteins and RNA [12]. Intriguingly, cigarette smoke-induced microRNA-21 (miR-21) expression has been suggested to amplify inflammatory responses and tumorigenesis processes in airway epithelial cells [13]. The latest data showed that miR-21 knockout suppressed airway hyper-responsiveness (AHR) and inflammation in the ovalbumin (OVA)-sensitized and -challenged mouse model [14]. Thus, the intention of this research was to characterize the anti-inflammatory and antioxidant properties of miR-21 loaded by mast cells-derived EVs in mouse airway epithelial MIC-iCell-a006 cells and a mouse model with asthma.

### Materials and methods

#### *Ethics statement*

The study was ratified by the Animal Ethical Committee of the Shanghai Putuo District Liqun Hospital (approval number: 20190023). All procedures were conducted according to the Guide for the Care and Use of Laboratory Animals published by the National Institutes of Health (NIH, Bethesda, Maryland, USA).

#### *Cell culture conditions*

Mouse airway epithelial cells (MIC-iCell-a006, iCell Bioscience Inc, Shanghai, China) were cultured with RPMI-1640 medium containing 0.1% penicillin, 0.1% streptomycin (Thermo Fisher Scientific Inc., Waltham, MA, USA) and 10% FBS. miR-21 inhibitor, small interfering RNA (si)-DDAH1 and negative control were

delivered into MIC-iCell-a006 cells with the help of Lipofectamine 3000 (Thermo Fisher Scientific). The plasmid vectors used were pCMV-MYC plasmid (Promega Corporation, Madison, WI, USA), and all sequences were synthesized by Gene Pharma (Shanghai, China). Totally,  $5 \times 10^5$  MIC-iCell-a006 cells were co-cultured with 50  $\mu\text{g}$  mast cells-derived EVs for 24 h for subsequent studies. When grown to 80-90% confluence, the cells were detached and plated into 6-well culture plates for adherence. A portion of cells were placed in an ozone chamber at 1.5 ppm for 2 h and then incubated at 37°C and 5% CO<sub>2</sub> for 24 h. For the control group, the cells were grown in a normal cell culture incubator. Serum-free RPMI-1640 medium was applied to prepare 20  $\mu\text{g}/\text{mL}$  lipopolysaccharide (LPS). The remaining cells were detached and incubated in this medium for 6 h. The control cells were induced with phosphate-buffered saline (PBS).

#### *Assessment of oxidative stress levels*

Determination of malondialdehyde (MDA) in cells and tissues of mice was conducted using a Lipid Peroxidation (MDA) Assay Kit (Sigma-Aldrich Chemical Company, St Louis, MO, USA). Totally, 10 mg tissue or  $1 \times 10^6$  cells was lysed using MDA containing 3  $\mu\text{L}$  butylated hydroxytoluene (100  $\times$ ) and centrifuged at 13,000 g for 10 min. The supernatant was incubated with 600  $\mu\text{L}$  tetrabutylammonium solution at 95°C for 60 min, and then the optical density (OD) value of the sample at A532 nm was determined by colorimetric method in a 96-well plate. The superoxide dismutase (SOD) determination kit (Sigma-Aldrich) was applied to assess the content of SOD in cells and tissues of mice. The samples were incubated with the mixture of 200  $\mu\text{L}$  water-soluble tetrazolium working solution, 20  $\mu\text{L}$  dilution buffer and 20  $\mu\text{L}$  enzyme working solution at 37°C for 20 min. A microplate reader (Elx800, BioTek Instruments, Winooski, VT, USA) was utilized to record the OD value at 450 nm.

#### *ELISA*

A mouse IL-13 ELISA Kit (ab219634, Abcam, Cambridge, UK), a mouse IL-5 ELISA Kit (Ousaid Biotechnology Co., Ltd., Changsha, Hunan, China), and a mouse IL-6 Quantikine ELISA Kit (R&D Systems, Minneapolis, MN, USA) were used to detect the levels of inflammatory fac-

## miR-21 derived from EVs promotes asthma

tors in mouse lung tissues. The antigen was ligated with a solid-phase carrier to form a solid-phase antigen, which was supplemented at 100  $\mu$ L/well and left overnight at 4°C in a 96-well plate. The cells were incubated with 150  $\mu$ L 1% bovine serum albumin solution for 1 h, with 100  $\mu$ L diluted serum for 2 h, and with 100  $\mu$ L diluted antibodies for 1 h (all at 37°C). OD values at A450 were read on a microplate reader (Elx800, BioTek) after 20 min of color development.

### *Microarray analysis*

Probes were resuscitated in 50 mM SpotArray 24 Microarray Printing System (PerkinElmer, MA, USA). The RNA was extracted by Trizol method (Thermo Fisher Scientific), and the reverse transcription reaction was implemented with random primers and AMV reverse transcriptase (Thermo Fisher Scientific) at 25°C for 10 min, at 40°C for 60 min, and at 70°C for 10 min. The cDNA was amplified by PCR, and the miRNA was labeled with Cy3. The PCR product containing the probe was hybridized with hybridization buffer (Ambion, Austin, TX, USA) overnight at 42°C and scanned with ScanArray Express Microarray Scanner (PerkinElmer). Scanned data were run on ScanArray Express version 1.0, and the spots with expression levels below 300 were excluded. miRNAs with at least 2-fold difference in expression were selected to plot the heatmap.

### *RT-qPCR*

TRIzol (Thermo Fisher Scientific) was applied to isolate the total RNA in accordance with the manufacturer's protocol. Random primers and AMV reverse transcriptase (Thermo Fisher Scientific) were applied at 25°C for 10 min, at 40°C for 60 min, and at 70°C for 10 min for reverse transcription, followed by primers and Taqman probe (Thermo Fisher Scientific) for quantitative RT-PCR reaction. Taqman probes were labeled with the fluorescent reporter group 6-carboxy-fluorescein at the 5' end and with the fluorescence-quenching group tetramethylrhodamine at the 3' end, with  $\beta$ -actin and GAPDH as the respective loading control. Primers for the quantitative PCR reaction were as follows: miR-21 forward, 5'-GCGCGCGTAGCTTATCAGACTGA-3'; reverse, 5'-ATCCAGTGCA-GGGTCCGAGG-3'; U6 forward, 5'-TCGCTTCGG-CAGCACATATACT-3'; reverse, 5'-ACGCTTCACG-AATTTGCGTGTC-3'; DDAH1 forward, 5'-GCCT-

GATGACATAGCAGCAA-3'; reverse, 5'-CCATCCACCTTTTCCAGTTC-3'; GAPDH forward, 5'-AGGTCGGTGTGAACGGATTTG-3'; reverse, 5'-TGTAG-ACCATGTAGTTGAGGTCA-3'.

### *Extraction and identification of EVs*

Mouse mast cells MC/9 (ATCC, Manassas, VA, USA) were starved for 12 h (without FBS) after incubating the cells to a steady state. Cells were harvested after a 300 g centrifugation for 10 min at 4°C and a 20,000 g centrifugation for 20 min, and the supernatant was filtered through a 0.2-mm filter and centrifuged again at 100,000 g for 1.5 h at 4°C to obtain EVs. The precipitate was resuspended with PBS, and the morphology of EVs was examined by TEM using a CM 10 Philips (Thermo Fisher Scientific). The number and size of EVs were determined using a NanoSight NS300 NTA (Malvern Panalytical, Malvern, UK). Expression of surface markers of EVs, including HSP70, CD9 and TSG101 was examined by western blot.

### *CCK-8 assay*

The transfected cells were evenly plated in a 96-well plate at  $5 \times 10^3$  cells/well and grown at 37°C with 5% CO<sub>2</sub> for indicated time. CCK-8 solution (10  $\mu$ L, Sigma-Aldrich) was added to each well for 2 h incubation at 37°C. OD value of cells at 450 nm was recorded by a microplate reader (Elx800, BioTek). Cell-free medium was used as a blank control to calculate cell proliferation.

### *Scratch assay*

Under aseptic conditions, scratches across the wells were made in a 6-well plate at intervals of 0.5-1 cm, and  $5 \times 10^5$  cells were seeded into the wells and cultured for 12 h. The cells were rinsed three times with PBS and cultured in RPMI-1640 medium containing 5% FBS at 37°C and 5% CO<sub>2</sub>. After 24 h, the samples were harvested and photographed. The width of the scratch was determined using Image J (NIH, Bethesda, MD, USA), and the cell migration capacity was evaluated by comparing the healing rate of the scratches. Scratch healing rate = (0-hour scratch width - 24-hour scratch width)/0-hour scratch width  $\times$  100%.

### *Transwell assay for cell invasion*

Matrigel (BD Biosciences, San Jose, CA, USA) was plated to the apical chamber under sterile

## miR-21 derived from EVs promotes asthma

conditions and incubated for 0.5 h. RPMI-1640 medium (30  $\mu$ L) was added to the apical chamber and placed in a CO<sub>2</sub> incubator, and the transfected cells were resuspended into a cell suspension (5  $\times$  10<sup>5</sup> cells/mL). RPMI-1640 medium with 10% FBS (500  $\mu$ L) was added to the basolateral chamber and 200  $\mu$ L cell suspension to the apical chamber for a 2 d incubation at 37°C in a 5% CO<sub>2</sub> incubator. The harvested cells were stained with crystal violet for 10 min, and then the number of invaded cells was counted under a microscope (Olympus Optical Co., Ltd., Tokyo, Japan).

### *Animals and experimental design*

Forty adult male SD mice were randomly allocated into eight groups (n = 5 in each): the saline group, the OVA group, the OVA + dimethylsulfoxide (DMSO) group, the OVA + EVs group, miR-21 control (OVA + EVs + miR-21 control), miR-21 inhibitor (OVA + EVs + miR-21 inhibitor), miR-21 inhibitor + DDAH1-NC (OVA + EVs + miR-21 inhibitor + DDAH1-NC), and miR-21 inhibitor + si-DDAH1 (OVA + EVs + miR-21 inhibitor + si-DDAH1). At the 7<sup>th</sup> d after EVs and plasmids injection, 35 mice were intraperitoneally injected with 50  $\mu$ g OVA solution (Sigma-Aldrich) and 1 mg aluminum hydroxide (Sigma-Aldrich) for sensitization, and the injection was repeated 7 d later. Inhalation started with ultrasonic nebulization with 1% OVA solution for 20 min on the 21<sup>st</sup> day for 3 consecutive days. Mice in the saline group (n = 5) were injected and inhaled with equal amounts of saline. A small animal respiratory function analysis system was used to detect pulmonary resistance (RL), and lung lavage fluid was collected for cell counting. Lung histopathological sections were observed to determine the success of the model, and lentiviral vectors and transfected fragments were synthesized by GenePharma (Shanghai, China).

### *Mouse lung function test*

Mice were subjected to an intraperitoneal injection of pentobarbital sodium (90 mg/kg) and then underwent tracheal intubation. Mice were placed in Whole Body Plethysmography (Data sciences international, St. Paul, MN, USA) and connected to a systemic air flow meter and pressure transducer. A small animal ventilator (Harvard Small Animal Ventilator Model 683, Harvard Apparatus, South Natick, MA, USA)

was used for mechanical ventilation with a tidal volume of 5-6 mL/kg at a frequency of 90 breaths/minute and a positive end-expiratory pressure of -8 cm H<sub>2</sub>O (1 cm H<sub>2</sub>O = 0.1098 kPa). The trans-pulmonary pressure, flow velocity and tidal volume were recorded as the baseline when the concentration of acetylcholine was zero (i.e., only saline was inhaled). Then, 10  $\mu$ L acetylcholine (gradient concentration, Sigma-Aldrich) was aerosolized to record changes in trans-pulmonary pressure and airway velocity within 3 min. AHR (airway hyper-responsiveness) is expressed as RL (lung resistance) (derived from multivariate linear regression of trans-pulmonary pressure and airflow), and the degree of AHR is expressed as the percentage of the peak value of each histamine inhalation dose to the saline value (variability in ventilatory function).

### *Analysis of tracheal inflammation*

The animals were euthanized by intraperitoneal injection of 1% sodium pentobarbital at 150 mg/kg after measurement of RL. Bronchoalveolar lavage (BAL) fluid was withdrawn after instillation of 1 mL sterile saline through trachea into the lung at 37°C for three times. After centrifugation at 1,500 rpm and 4°C for 5 min, the cell precipitate was then suspended with PBS and centrifuged at 1,500 rpm and 4°C for 5 min. Giemsa stain (Beijing Solabio Life Sciences Co., Ltd., Beijing, China) was supplemented to sort the cells and measure the number of BAL cells, eosinophils, neutrophils, macrophages and lymphocytes in the trachea under a light microscope (Olympus).

### *HE staining*

After euthanasia of the mice, the lung tissues were removed and fixed in neutral formaldehyde solution (10%) for 1 d. Afterwards, the tissues were dehydrated with 70%, 80%, 90%, 95% and 100% ethanol, cleared with xylene, embedded in paraffin, and cut into 5- $\mu$ m sections. After a 4-min hematoxylin (Solarbio) staining, the sections were differentiated in ethanol hydrochloric acid for 10 s, rinsed, stained again with eosin (Solarbio) for 2 min, fixed with neutral gum, and viewed for damage and inflammatory cell infiltration in lung tissues under a DMM-300D microscope (Shanghai CaiKon Optical Instrument Co., Ltd., Shanghai, China).

## miR-21 derived from EVs promotes asthma

### Dual-luciferase experiment

The bioinformatics websites StarBase (<http://starbase.sysu.edu.cn/>), miRanda (<http://www.microrna.org/>), miRDB (<http://www.mirdb.org/>), and Targetscan (<http://www.targetscan.org/>) were utilized to analyze the target genes of miR-21. The binding relation between DDAH1 and miR-21 was examined by dual-luciferase reporter gene analysis. Complementary sequences and mutation sites were designed based on predictions. The target fragments were subcloned into the pMIR-reporter plasmids (Addgen, Cambridge, MA, USA) using T4 DNA ligase (Takara Biotechnology Ltd., Dalian, Liaoning, China). The luciferase reporter plasmids wild-type (WT) and mutant (MT) were delivered with miR-21 into HEK-293T cells (ATCC), respectively. The cells were collected by centrifugation for 3 min after incubation at 37°C for 48 h. Firefly luciferase assay Kit and Renilla luciferase assay Kit (Beyotime, Shanghai, China) were applied. After the addition of 100 µL buffer (1:100) into 100 µL sample, the relative light unit (RLU) value was measured with the cell lysate of the reporter gene served as a blank control. Luciferase activity was calculated as RLU values from the firefly luciferase assay and RLU values from the Renilla luciferase assay.

### Western blot

Cells and tissues were lysed using pre-chilled 1 × lysis buffer (Thermo Fisher Scientific) for 10 min. The proteins were obtained by centrifugation and measured by a bicinchoninic acid assay protein quantification kit. An equal amount of total protein was taken from each sample for SDS-PAGE and transferred to a PVDF membrane (Millipore Corp, Billerica, MA, USA) by transfer electrophoresis device (Bio-Rad, Inc., Hercules, CA, USA). After sealing with 5% non-fat dry milk for 60 min, the PVDF membrane was probed with primary antibodies to β-catenin (1:500, sc-7963, Santa Cruz Biotechnology Inc., Santa Cruz, CA, USA), cyclin D1 (1:500, sc-8396, Santa Cruz Biotechnology), GAPDH (1:2000, ab8245), HSP70 (#4873, 1:1000, Cell Signaling Technologies, Beverly, MA, USA), CD9 (#13403, 1:1000, Cell Signaling Technologies), and TSG101 (1:1000, ab83, Abcam) overnight at 4°C. PVDF membranes were then re-probed with HRP-labeled second-

ary antibody (1:5000, ab205719, Abcam) for 2 h at ambient temperature. Protein expression was quantified by colorimetric reaction using ECL plus western blotting system reagent kit (Solarbio). The original blots are presented in the [Supplementary Materials](#).

### Data analysis

SPSS (v22.0, IBM SPSS Statistics, Chicago, IL, USA) was applied for statistical analysis. The bioinformatics images were plotted using R software ([www.r-project.org](http://www.r-project.org)), and the statistical graphs were drawn using Graph Prism 8 (GraphPad, San Diego, CA, USA). Data were expressed as mean ± SD and analyzed by one-way or two-way ANOVA, followed by Tukey's multiple range tests or unpaired *t* test. *P* < 0.05 was deemed as statistically significant.

## Results

### *miR-21 is highly expressed in ozone- and LPS-induced airway epithelial cells*

To investigate the molecular mechanisms of airway epithelial cells during stress and inflammation, we first developed an *in vitro* airway epithelial cell model of oxidative stress and inflammation. In order to verify the success of the oxidative stress model, we examined the oxidative stress under the ozone induction and found that the MDA level in the cells increased significantly, whereas SOD level decreased, indicating increased oxidative stress (**Figure 1A**). After that, we induced cellular inflammation by LPS. LPS (20 µg/mL)-treated cells were collected, and the levels of pro-inflammatory factors IL-5, IL-6 and IL-13 were examined by ELISA, which were significantly enhanced (**Figure 1B**). We then extracted RNA from ozone-induced cells and LPS-treated cells and performed miRNA microarray analysis (**Figure 1C, 1D**). After comparing the two microarray results, miR-21 was found to be over-expressed in both models under conditions of oxidative stress and inflammation *in vitro*, with the most significant change (**Figure 1E**). Our evaluation of miR-21 expression in ozone-induced and LPS-treated cells validated this result (**Figure 1F**). This suggests that miR-21 may be a factor in the development of oxidative stress and inflammation in airway epithelial cells.

## miR-21 derived from EVs promotes asthma

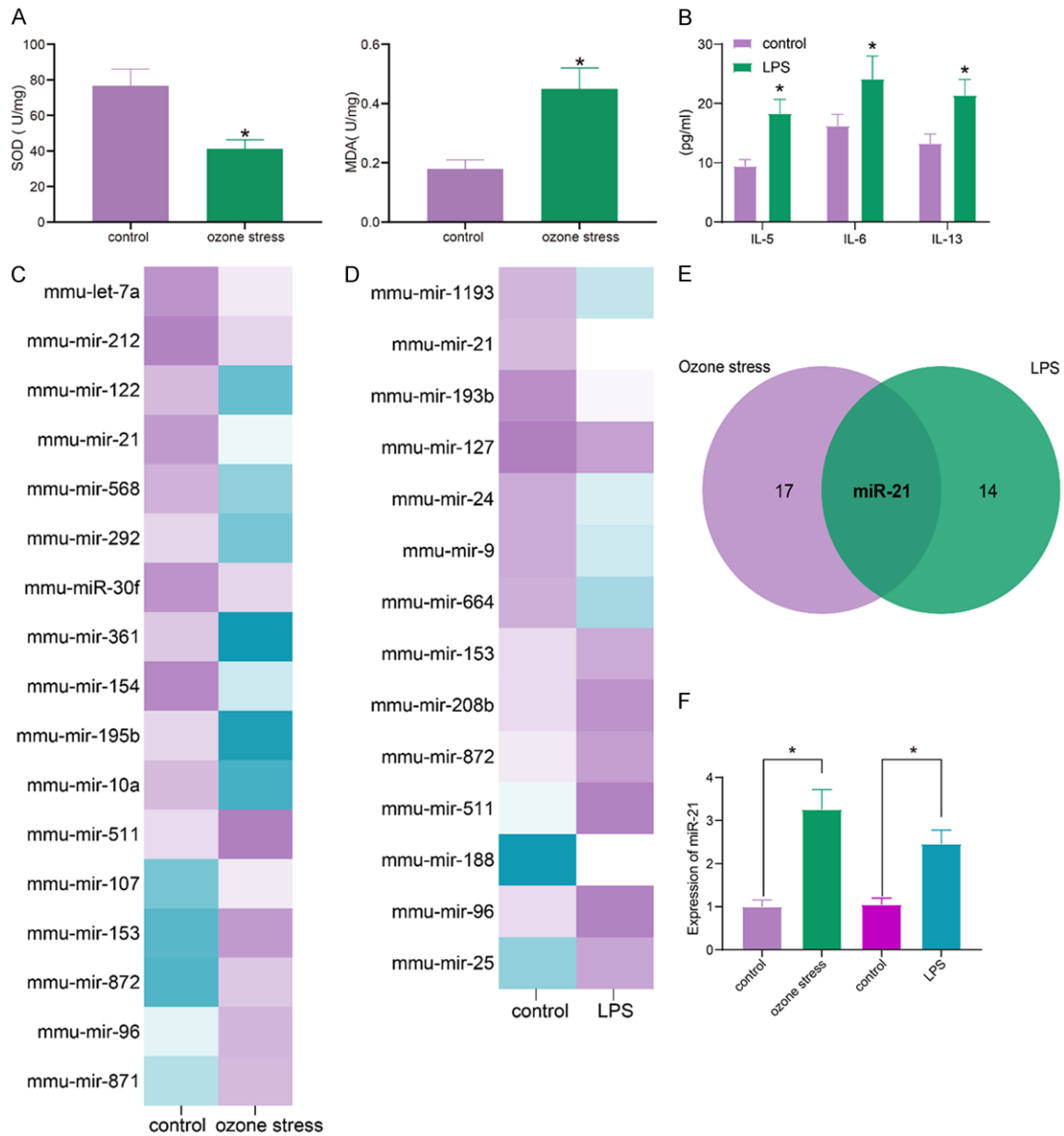


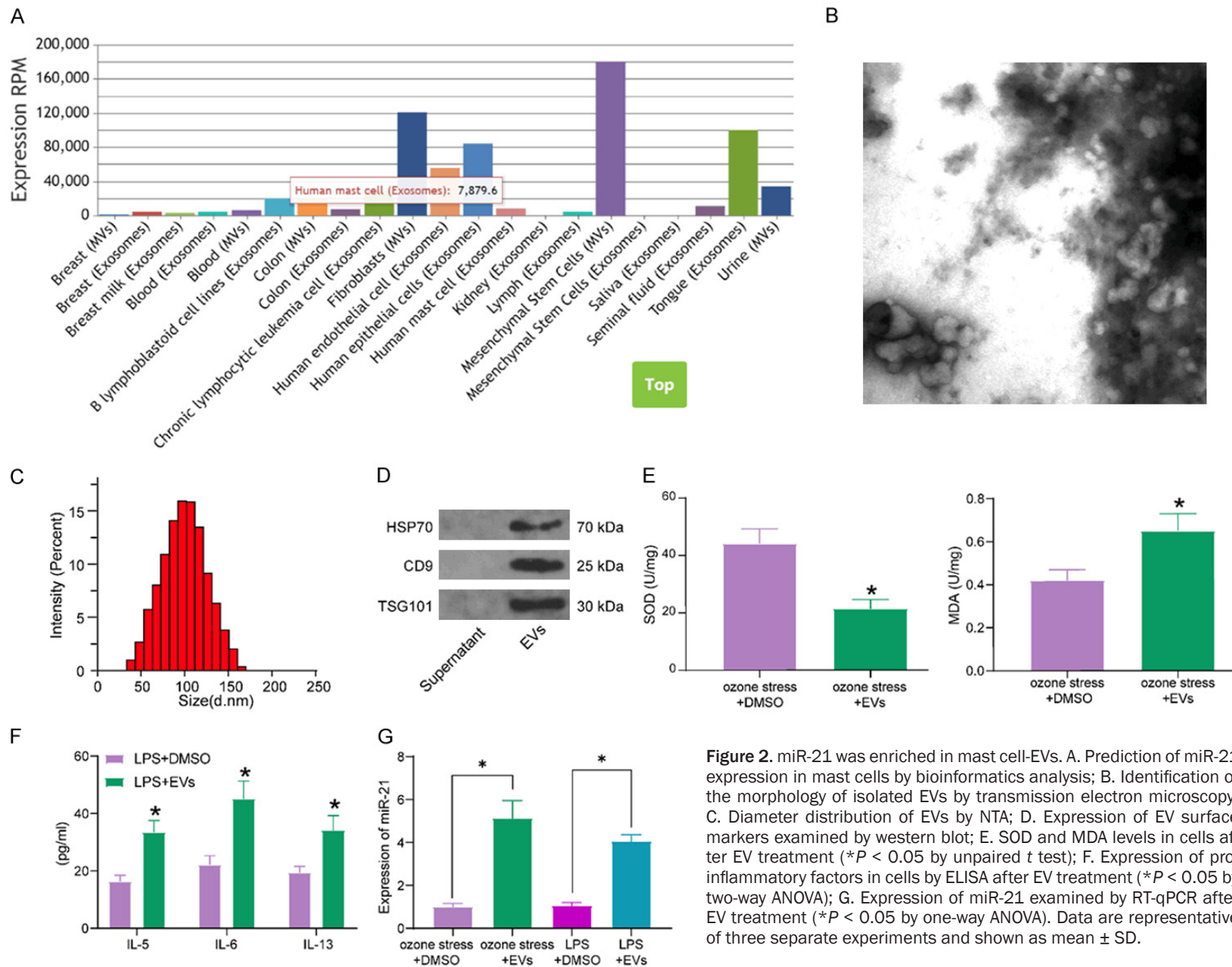
**Figure 1.** miR-21 was highly expressed in airway epithelial cells exposed to ozone or LPS. A. Detection of changes in SOD and MDA levels in cells exposed to ozone ( $*P < 0.05$  by unpaired *t* test); B. Detection of changes in IL-5, IL-6 and IL-13 levels in cells exposed to LPS ( $*P < 0.05$  by two-way ANOVA); C. Altered miRNAs in cells exposed to ozone by miRNA microarray analysis; D. Altered miRNAs in cells exposed to LPS by miRNA microarray analysis; E. Venn map screening for miRNAs expressed highly both in cells exposed to ozone and LPS; F. miR-21 expression in cells by RT-qPCR ( $*P < 0.05$  by one-way ANOVA). Data are representative of three separate experiments and shown as mean  $\pm$  SD.

### miR-21 is present in mast cells-derived EVs

Inquiry using the EVmiRNA website (<http://bioinfo.life.hust.edu.cn/EVmiRNA/#/>) revealed that miR-21 was mainly presented in mast cells (Figure 2A). We extracted EVs from mast cells by centrifugation and observed that the

shape of EVs was elliptical under transmission electron microscopy (Figure 2B). The diameter of EVs was analyzed by NTA and found to be in the range of 30-150 nm, which was in accordance with the definition of EVs (Figure 2C). Also, the expression of HSP70, CD9 and TSG101 was positive for the extracted EVs, as

## miR-21 derived from EVs promotes asthma



manifested by western blot (**Figure 2D**). So far, we have successfully isolated mast cell-EVs. EVs were co-cultured with ozone-induced cells or LPS-treated cells, and the changes of cell activity were detected. The expression of SOD was significantly reduced, and MDA expression was increased, suggesting promoted oxidative stress after EV treatment (**Figure 2E**). After EV treatment of inflammatory cells, the levels of IL-5, IL-6 and IL-13 were significantly increased, and the inflammatory response in the cells was enhanced (**Figure 2F**). Finally, the expression changes of miR-21 in both cells before and after EV treatment were examined by RT-qPCR. We found that the miR-21 expression was significantly increased in both cells after EV treatment (**Figure 2G**). Therefore, we assumed that miR-21, contained in mast cells-derived EVs, was delivered to mouse airway epithelial cells by EVs to promote oxidative stress and inflammatory responses.

### *Mast cells-derived EVs regulate oxidative stress and inflammatory responses via miR-21*

To test the aforementioned conjecture, we inhibited miR-21 expression by transfection of miR-21 inhibitor in two EVs-treated airway epithelial cell models and verified the transfection efficiency by PCR (**Figure 3A**). CCK-8 assays were conducted to evaluate OD values in cells with suppressed miR-21 expression. The proliferative activity of both cells was significantly enhanced after miR-21 down-regulation (**Figure 3B**). Subsequently, changes in cell migration capacity were detected by scratch assay, and migration capacity was significantly increased in airway epithelial cells after miR-21 inhibitor transfection (**Figure 3C**). Detection of differences in cell invasion activity by Transwell experiments revealed that miR-21 down-regulation enhanced invasive capacity in cells (**Figure 3D**). Finally, we evaluated the SOD and MDA levels in cells and found that oxidative stress was hampered after miR-21 down-regulation (**Figure 3E**). Quantitative analysis of the levels of the IL-5, IL-6 and IL-13 in cells revealed that down-regulation of miR-21 decreased cellular inflammatory factors (**Figure 3F**). This series of experiments verified that inhibition of miR-21 increased airway epithelial cell activity and attenuated the oxidative stress and inflammatory responses.

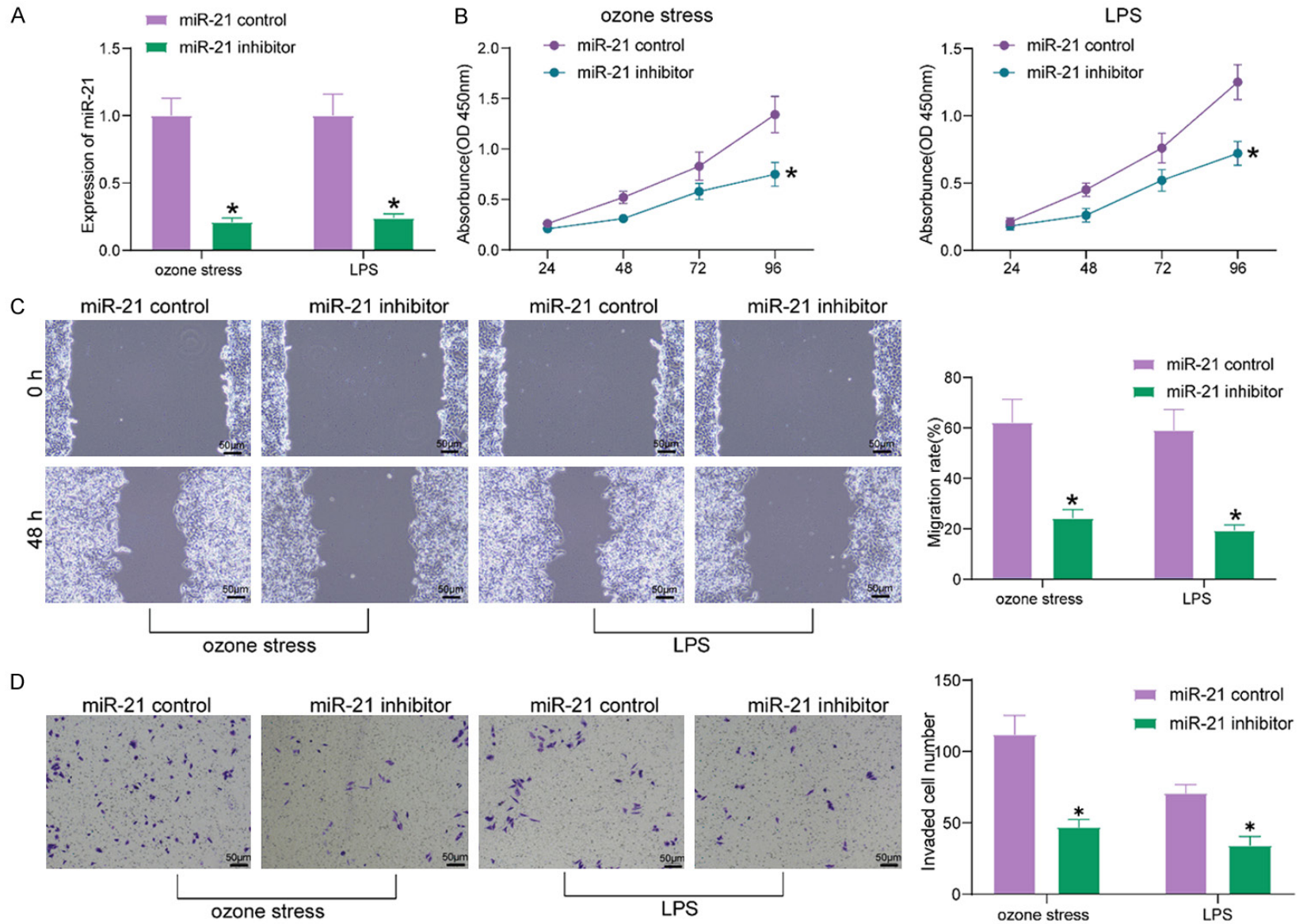
### *miR-21 is highly expressed in OVA-challenged asthmatic mice*

In order to verify the success of the asthma mouse model, we stained the lung tissues of the mice using HE staining, which showed that the bronchial walls and alveoli of the mice treated with saline were intact, with regular shape and free of narrowing of the lumen. In the OVA-challenged mice, there were obvious signs of bronchoconstriction and inflammatory cell infiltration around the small blood vessels, alveolar cavity and lung interstitium, and bronchial epithelial cell detachment, pulmonary arteriolar edema and respiratory bronchial obstruction (**Figure 4A**). The detection of AHR in mice revealed that asthmatic mice induced significant AHR, which was mainly manifested by a significant increase in RL after histamine inhalation (**Figure 4B**). Subsequently, BAL cell counts exhibited that airway inflammation was significantly augmented in asthmatic mice compared with saline-treated mice in terms of the counts of total BAL cells, eosinophils, neutrophils, macrophages and lymphocytes (**Figure 4C**). Finally, we noted that the levels of pro-inflammatory factors and MDA were significantly enhanced, while SOD levels were reduced (**Figure 4D, 4E**). The epithelial tissues of mouse airways were extracted, and the changes of miR-21 expression were detected using PCR quantification. miR-21 was found to be significantly up-regulated in the epithelial tissues of asthmatic mice (**Figure 4F**). This suggests that our asthmatic mouse model was successfully developed, and miR-21 was significantly over-expressed in this model.

### *Mast cells-derived EVs exacerbate oxidative stress and inflammatory responses in asthmatic mice via miR-21*

EVs extracted from mast cells were injected into asthmatic mice, and the miR-21 expression was remarkably elevated in airway tissues (**Figure 5A**). We then injected EVs-treated asthmatic mice with miR-21 inhibitor and validated the success of modeling by quantitative analysis of miR-21 expression in airway tissues (**Figure 5B**). The oxidative stress and inflammation in the airway tissues of mice after administration with miR-21 inhibitor and EVs were detected. First, AHR was assessed in the EVs-treated mice, and it was found that the

miR-21 derived from EVs promotes asthma



## miR-21 derived from EVs promotes asthma

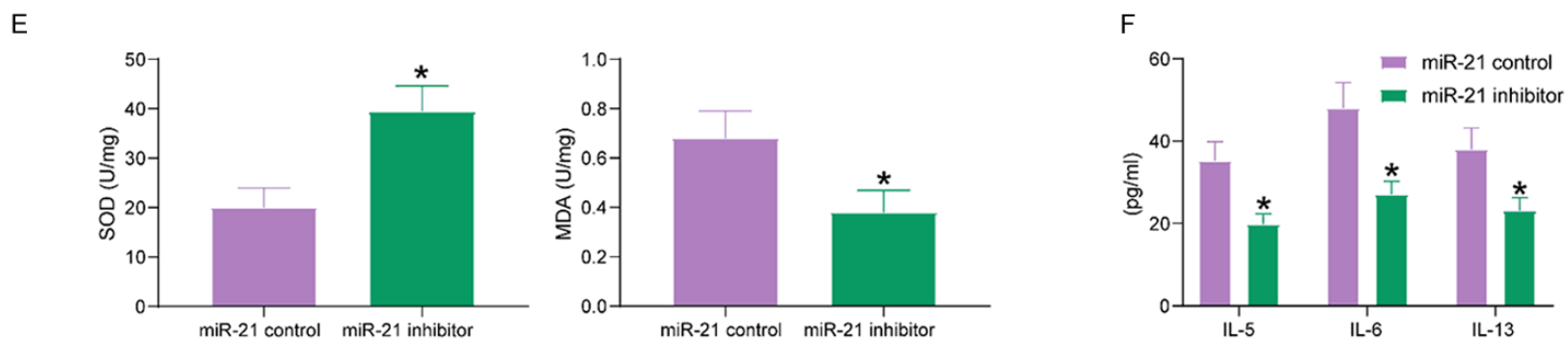
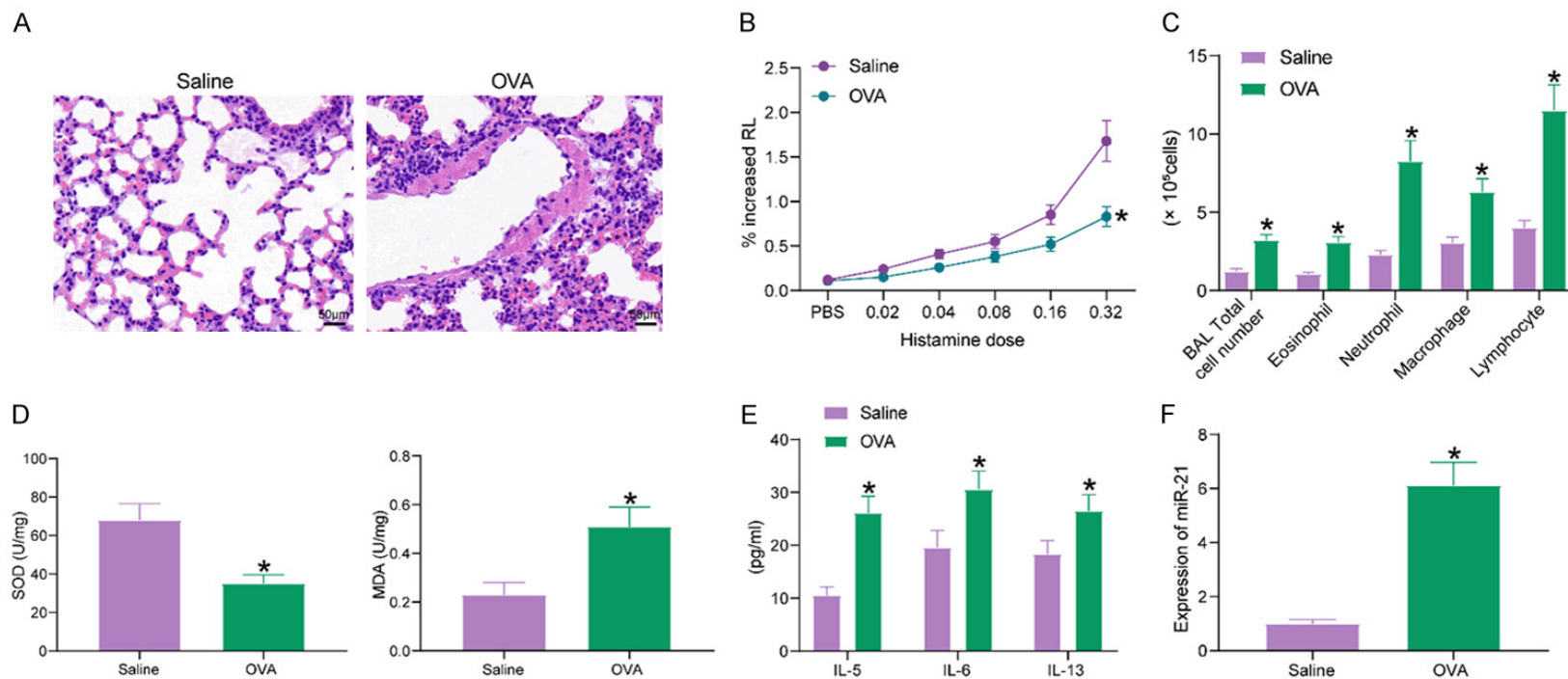


**Figure 3.** miR-21 inhibitor reduced oxidative stress and inflammatory responses in cells. miR-21 inhibitor or control was transfected into cells exposed to LPS or zone. A. Transfection efficacy of miR-21 inhibitor examined by RT-qPCR ( $*P < 0.05$  by the two-way ANOVA); B. Cell proliferation examined by CCK-8 assay ( $*P < 0.05$  by two-way ANOVA); C. Cell migration capacity examined by scratch assay ( $*P < 0.05$  by two-way ANOVA); D. Cell invasion activity assessed by Transwell assay ( $*P < 0.05$  by two-way ANOVA); E. SOD and MDA levels in cells were examined ( $*P < 0.05$  by unpaired *t* test); F. Expression of pro-inflammatory factors in cells by ELISA ( $*P < 0.05$  by two-way ANOVA). Data are representative of three separate experiments and shown as mean  $\pm$  SD.



## miR-21 derived from EVs promotes asthma

**Figure 4.** miR-21 was expressed highly in airway tissues of OVA-challenged asthmatic mouse model. A. HE staining of mouse lung tissue to assess the development of an asthmatic mouse model; B. Assessment of mouse airway stress by detection of AHR in mice ( $*P < 0.05$  by two-way ANOVA); C. Changes in inflammatory cell content in the airways of mice assessed by BAL cell count ( $*P < 0.05$  by two-way ANOVA); D. SOD and MDA levels in cells were examined ( $*P < 0.05$  by unpaired t test); E. Expression of pro-inflammatory factors in cells by ELISA ( $*P < 0.05$  by two-way ANOVA); F. Quantification of miR-21 expression in airway tissues of asthmatic mice by RT-qPCR ( $*P < 0.05$  by unpaired t test). Data are representative of three separate experiments ( $n = 5$ ) and shown as mean  $\pm$  SD.

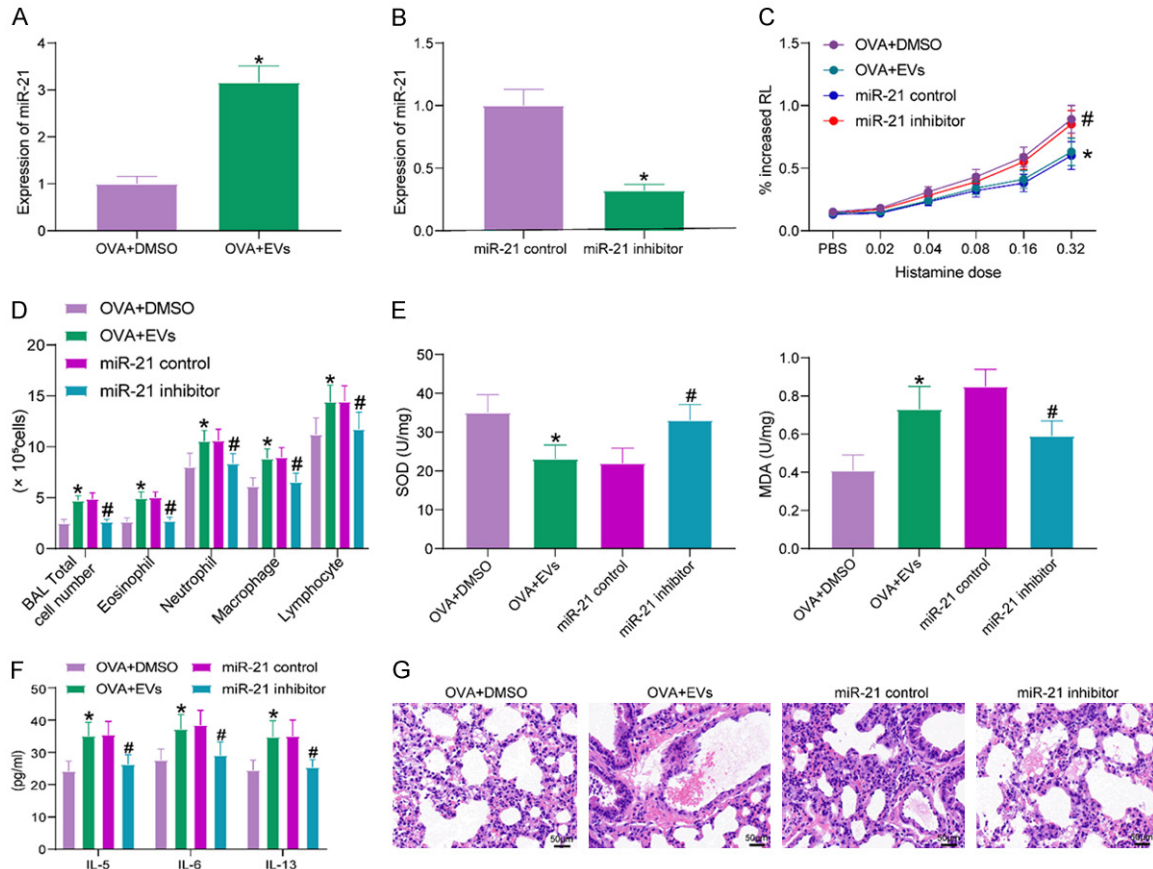


**Figure 5.** miR-21 inhibitor negated the stimulative role of mast cells-derived EVs in oxidative stress and inflammatory responses of OVA-sensitized asthmatic mouse model. Mice were treated with miR-21 inhibitor or miR-21 control in the presence of OVA or OVA alone ( $n = 5$ ). A. Quantification of miR-21 expression in airway tissues of asthmatic mice or mice treated with DMSO by RT-qPCR ( $*P < 0.05$  by unpaired t test); B. Quantification of miR-21 expression in airway tissues of asthmatic mice treated with miR-21 inhibitor or miR-21 control by RT-qPCR ( $*P < 0.05$  by unpaired t test); C. Changes in AHR levels in mice ( $*P < 0.05$  by two-way ANOVA); D. Changes in inflammatory cell content in mouse BAL fluid to assess airway inflammatory response in mice ( $*P < 0.05$  by two-way ANOVA); E. SOD and MDA levels in cells were examined ( $*P < 0.05$  by two-way ANOVA); F. Expression of pro-inflammatory factors in cells by ELISA ( $*P < 0.05$  by two-way ANOVA); G. HE staining for injury and inflammatory cell infiltration in the lung tissue of mice. Data are shown as mean  $\pm$  SD.

level of AHR in mice was enhanced after EVs treatment and repressed after down-regulation of miR-21 (Figure 5C). Moreover, mast cells-derived EVs induced increases in total BAL cell, eosinophil, neutrophil, macrophage and lymphocyte counts in mice, while miR-21 down-regulation decreased inflammatory cell infiltration in mice (Figure 5D). Detection of oxidative

stress levels in tissues revealed that EVs elevated oxidative stress in tissues, and miR-21 inhibitor reduced oxidative stress (Figure 5E). The pro-inflammatory factors IL-5, IL-6 and IL-13 in airway tissue were up-regulated by EV induction, while miR-21 inhibitor injection down-regulated the level of pro-inflammatory factors in mice (Figure 5F). Finally, we observed

lung injury in mice by HE staining and found that EVs worsened lung injury and bronchial obstruction. By contrast, down-regulation of miR-21 alleviated lung tissue injury, and bronchial obstruction became less pronounced with reduced inflammatory cell infiltration (**Figure 5G**). Through these experiments, we demonstrated that mast cell-EVs exacerbated oxidative stress and inflammation in asthmatic mice by carrying miR-21.

*miR-21 targets DDAH1 to mediate the Wnt/ $\beta$ -catenin pathway*

To probe the mechanism of miR-21 in oxidative stress and inflammation, the genes targeted by miR-21 were predicted by bioinformatics websites, and DDAH1 was found to be a possible target of miR-21 (**Figure 6A**). Examination of the expression of DDAH1 in cells revealed that DDAH1 was significantly down-regulated in both models under conditions of oxidative stress and inflammation *in vitro* (**Figure 6B**). Detection of the targeting relation between miR-21 and DDAH1 using a Dual-luciferase assay displayed that HEK293T cells transfected with miR-21 inhibitor and DDAH1-WT showed significantly increased luciferase intensity (**Figure 6C**). DDAH1 mRNA expression was then examined in cells with miR-21 inhibitor, which suggested that DDAH1 was significantly elevated after miR-21 down-regulation (**Figure 6D**). The efficiency was verified using RT-qPCR after simultaneous down-regulation of DDAH1 and miR-21 in cells and mice (**Figure 6E**). Western blot analysis in cells revealed a significant increase in Wnt/ $\beta$ -catenin pathway under conditions of oxidative stress and inflammation *in vitro* (**Figure 6F**). The Wnt/ $\beta$ -catenin pathway was then found to be activated after EV treatment, impaired in miR-21 low-expressing cells, and induced again in DDAH1 low-expressing cells (**Figure 6G**). The Wnt/ $\beta$ -catenin pathway was also expedited in asthmatic mice and blocked in miR-21 inhibitor-treated mice, which was further potentiated by DDAH1 knockdown (**Figure 6H**). These experiments demonstrated the involvement of the miR-21/DDAH1/Wnt/ $\beta$ -catenin axis in asthma.

*Knockdown of DDAH1 antagonizes the repressive effects of miR-21 inhibitor on oxidative stress and inflammation*

Detection of oxidative stress cells revealed that down-regulation of DDAH1 increased MDA lev-

els and diminished SOD levels in the presence of miR-21 inhibitor (**Figure 7A**). In LPS-pretreated cells, down-regulation of DDAH1 was found to increase the levels of pro-inflammatory factors in the cells with miR-21 knockdown (**Figure 7B**). Simultaneous knockdown of miR-21 and DDAH1 was also delivered into EV-treated asthmatic mice. After validation of DDAH1 knockdown in airway tissues (**Figure 7C**), detection of oxidative stress and inflammation in mouse airway tissues was carried out. Enhanced oxidative stress (**Figure 7D**) and inflammation (**Figure 7E**) were observed after miR-21 and DDAH1 inhibition. Finally, we identified the effects of miR-21 and DDAH1 inhibition on asthmatic mice by HE staining of their lung tissues, and found that down-regulation of DDAH1 exacerbated inflammatory infiltration, pulmonary arteriolar edema, and bronchial obstruction in mice even with the inhibition of miR-21 (**Figure 7F**).

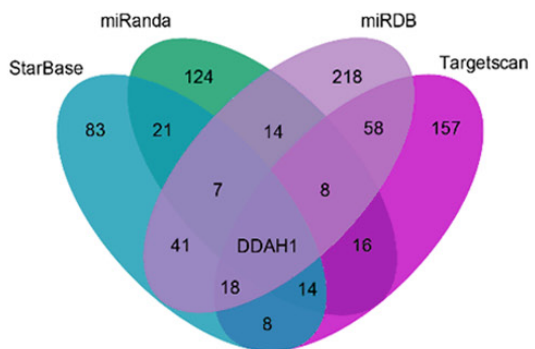
## Discussion

Asthma is a chronic inflammatory disease of the airways, which is evoked in the context of AHR recurrent wheezing, and clinical symptoms, including inflammation and AHR, could be sufficiently controlled in approximately 80% of asthmatics with daily medication [15]. Still, it is of paramount importance to assess epithelial abnormalities to elicit clinical benefits for epithelial-directed therapies. The present study demonstrated that in ozone and LPS exposure cell models and in OVA-sanitized mouse model, miR-21 released from mast cell-EVs promoted airway inflammation and oxidative stress, which were associated with promotion of BAL cell counts and cytokine levels, and suppression of airway epithelial cell activities. Knockdown of DDAH1, a target of miR-21, increased MDA and cytokine levels via the Wnt/ $\beta$ -catenin signaling activity. These data imply that miR-21 released from mast cell-EVs induces airway inflammation and oxidative stress at least in part through reducing DDAH1 and activating the Wnt/ $\beta$ -catenin signaling.

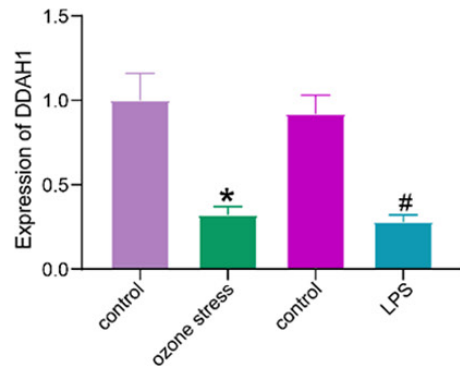
EVs have been suggested to play an important part for the function of mast cells, and transcriptome analysis of mast cell-derived EVs might shed lights on the regulatory functions of mast cells and mast cell-derived EVs [16]. As a consequence, we performed microarray analyses on two established cells exposed to LPS and ozone. It was found that miR-21 was the

# miR-21 derived from EVs promotes asthma

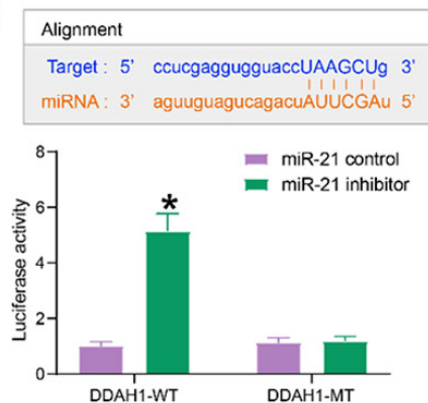
A



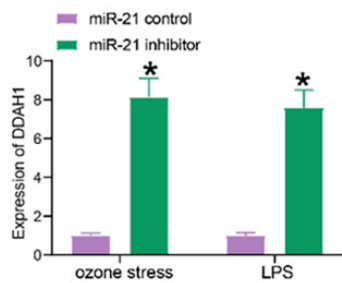
B



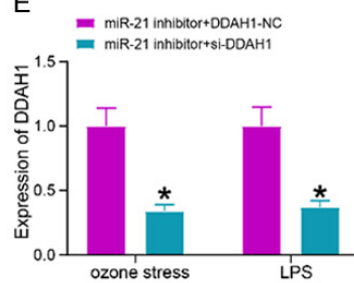
C



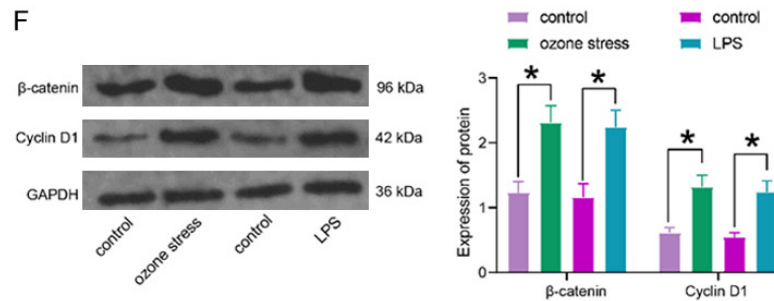
D



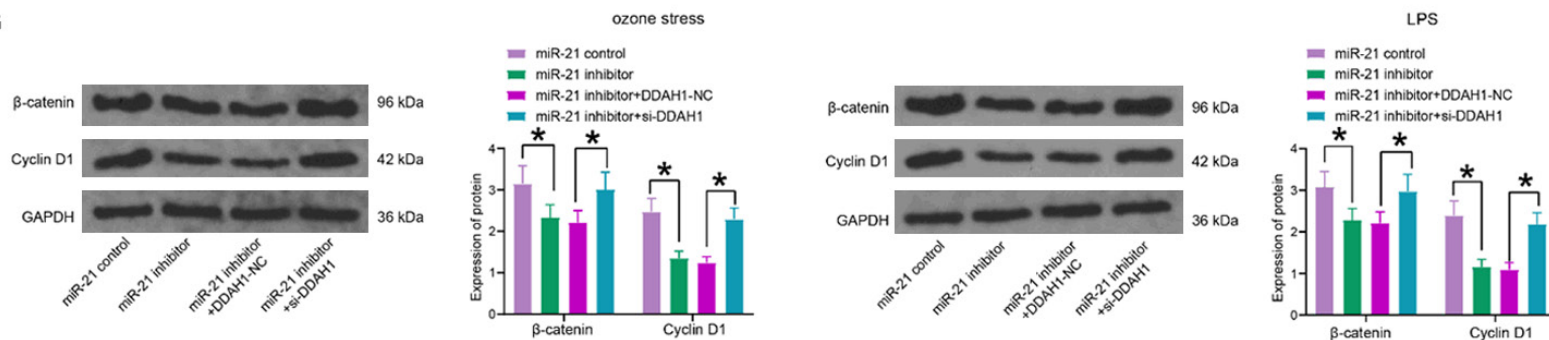
E



F



G



## miR-21 derived from EVs promotes asthma

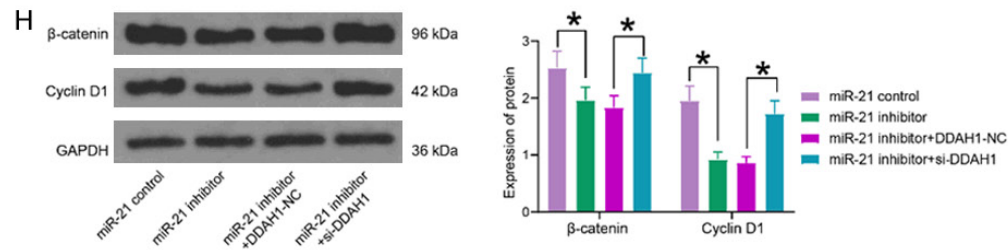


**Figure 6.** DDAH1/Wnt/ $\beta$ -catenin axis was identified as the downstream signaling of miR-21 in asthma. A. Venn map screening of miR-21 target genes; B. DDAH1 expression in ozone- and LPS-treated cells ( $*P < 0.05$  by one-way ANOVA); C. The relationship between miR-21 and DDAH1 examined by dual-luciferase assay ( $*P < 0.05$  by two-way ANOVA); D. DDAH1 expression in miR-21 down-regulated cells ( $*P < 0.05$  by one-way ANOVA); E. DDAH1 expression in DDAH1 down-regulated cells ( $*P < 0.05$  by one-way ANOVA); F.  $\beta$ -catenin and cyclin D1 protein expression in ozone- and LPS-induced cells ( $*P < 0.05$  by two-way ANOVA); G.  $\beta$ -catenin and cyclin D1 protein expression in cells after co-transfection in the presence of LPS or ozone ( $*P < 0.05$  by two-way ANOVA); H.  $\beta$ -catenin and cyclin D1 protein expression in airway tissues of mice after delivery ( $*P < 0.05$  by two-way ANOVA). Data are representative of three separate experiments ( $n = 5$ ) and shown as mean  $\pm$  SD.

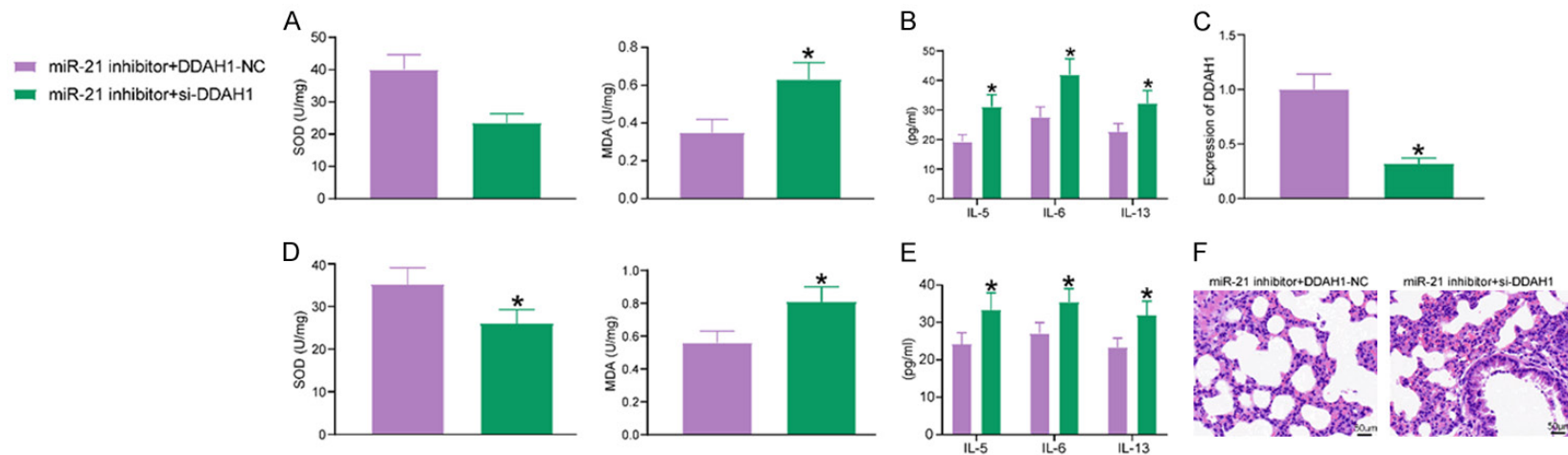


**Figure 7.** DDAH1 knockdown reversed the alleviating effects of miR-21 inhibitor on oxidative stress and inflammatory responses. Cells exposed to LPS or ozone and mice treated with OVA were delivered with miR-21 inhibitor + si-DDAH1 or miR-21 inhibitor + DDAH1-NC. A. SOD and MDA levels in ozone-exposed cells ( $*P < 0.05$  by one-way ANOVA); B. Expression of pro-inflammatory factors in cells by ELISA ( $*P < 0.05$  by two-way ANOVA); C. Quantification of DDAH1 expression in airway tissues of asthmatic mice by RT-qPCR ( $*P < 0.05$  by one-way ANOVA); D. SOD and MDA levels in airway tissues of asthmatic mice ( $*P < 0.05$  by two-way ANOVA); E. Expression of pro-inflammatory factors in airway tissues of asthmatic mice by ELISA ( $*P < 0.05$  by two-way ANOVA); F. HE staining for injury and inflammatory infiltration in lung tissue. Data are representative of three separate experiments ( $n = 5$ ) and shown as mean  $\pm$  SD.

only miRNA expressed highly in both cells. Consistently, Elbehidy *et al.* reported that serum miRNA-21 was much higher in the asthmatic children, which could be a potential biomarker for the diagnosis and therapy of asthma [17, 18]. Moreover, integrated bioinformatics website prediction and functional assays revealed that the up-regulation of miR-21 in airway epithelial cells may be due the delivery of mast cell-EVs. For further validation, we knocked down miR-21 expression using miR-21 inhibitor. It was noted that miR-21 inhibitor remarkably enhanced airway epithelial cell proliferation, migration and invasion. In addition, depletion of miR-21 suppressed airway inflammation and oxidative stress in both airway epithelial cells and airway tissues of mice. miR-21 has been displayed to elevate inflammatory mediators in non-hematopoietic cells, contributing to neoplastic transformation [19]. Likewise, paraquat enhanced miR-21 and oxidative stress in the lungs, while radix puerariae extracts reduced oxidative stress through decreasing expression of miR-21 [20]. It has been established by that a cascade of immune responses caused by inhaled LPS led to Th2 cell induction, whereas IL-5 and IL-13 released by Th2 cells resulted in asthma progression [21]. Lee *et al.* presented that miR-21 antagomir suppressed AHR versus the OVA-challenged and scrambled RNA-treated BALB/c mice, diminished the total cell and eosinophil counts in BAL fluid, and the expression profile of IL-5 and IL-13 [22]. Subsequently, we sought to decipher the mechanism of miR-21 in asthma, several bioinformatics websites were utilized to screen out DDAH1 as a putative target of miR-21. DDAH1 3'UTR has been verified as a putative target for miR-21, and endogenous miR-21 decreased the expression of DDAH1 transcript in human umbilical venous endothelial cells [23]. Previously, Kinker *et al.* proposed that decreased expression of DDAH1 led to allergic asthma, and DDAH1 up-regulation attenuated allergen-induced airway inflammation via modulating Th2 responses [24]. In addition, deficiency of DDAH1 promoted intracellular oxidative stress and apoptosis through a miR-21-dependent manner in mouse embryonic fibroblasts [25]. Moreover, miR-21 was revealed to facilitate renal fibrosis by the Wnt pathway via targeting DDAH1 [26]. Thus, we wondered whether miR-21 also regulated the airway inflammation and oxidative stress processes in

asthma via the DDAH1/Wnt/ $\beta$ -catenin axis. Our western blot validated our conjecture by providing evidence that the expression of  $\beta$ -catenin and cyclin D was significantly induced in airway tissues of asthmatic mice and cells exposed to LPS and ozone, while impaired after miR-21 inhibitor and activated again following DDAH1 knockdown. Our subsequent rescue experiments further substantiated the involvement of DDAH1 in miR-21-mediated airway inflammation and oxidative stress.

### Conclusion

In summary, our *in vitro* studies illustrate that miR-21 loaded by mast cells-derived EVs can regulate intracellular inflammation and oxidative stress by attenuating DDAH1 expression in LPS- and ozone-stimulated airway epithelial cells. Moreover, the results of the *in vivo* studies provide clear evidence for the anti-inflammatory and antioxidant activity of miR-21 inhibitor. These data might provide experimental support for the therapeutic application of miR-21 inhibitor and mast cells-derived EVs against asthma. Mouse mast cells were used as the study model, and the species-specific differences between mouse mast cells and human mast cells might hinder the therapeutic application of mast cells-derived EVs, which constitute the limitation of the present study.

### Disclosure of conflict of interest

None.

**Address correspondence to:** Ying Zou, Department of Respiratory and Critical Medical, Shanghai Putuo District Liqun Hospital, No. 910, Taopu Road, Shanghai 200333, P. R. China. Tel: +86-021-52780030; Fax: +86-021-52780030; E-mail: zouying\_729@163.com

### References

- [1] Lambrecht BN and Hammad H. The airway epithelium in asthma. *Nat Med* 2012; 18: 684-692.
- [2] Grainge CL and Davies DE. Epithelial injury and repair in airways diseases. *Chest* 2013; 144: 1906-1912.
- [3] Chung KF and Marwick JA. Molecular mechanisms of oxidative stress in airways and lungs with reference to asthma and chronic obstructive pulmonary disease. *Ann N Y Acad Sci* 2010; 1203: 85-91.

## miR-21 derived from EVs promotes asthma

- [4] Zhang P, Li F, Wiegman CH, Zhang M, Hong Y, Gong J, Chang Y, Zhang JJ, Adcock I, Chung KF and Zhou X. Inhibitory effect of hydrogen sulfide on ozone-induced airway inflammation, oxidative stress, and bronchial hyperresponsiveness. *Am J Respir Cell Mol Biol* 2015; 52: 129-137.
- [5] Matsuguchi T. Mast cells as critical effectors of host immune defense against Gram-negative bacteria. *Curr Med Chem* 2012; 19: 1432-1442.
- [6] Rodewald HR and Feyerabend TB. Widespread immunological functions of mast cells: fact or fiction? *Immunity* 2012; 37: 13-24.
- [7] Carroll-Portillo A, Surviladze Z, Cambi A, Lidke DS and Wilson BS. Mast cell synapses and exosomes: membrane contacts for information exchange. *Front Immunol* 2012; 3: 46.
- [8] Yáñez-Mó M, Siljander PR, Andreu Z, Zavec AB, Borrás FE, Buzas EI, Buzas K, Casal E, Cappello F, Carvalho J, Colás E, Cordeiro-da Silva A, Fais S, Falcon-Perez JM, Ghobrial IM, Giebel B, Gimona M, Graner M, Gursel I, Gursel M, Heegaard NH, Hendrix A, Kierulf P, Kokubun K, Kosanovic M, Kralj-Iglic V, Krämer-Albers EM, Laitinen S, Lässer C, Lener T, Ligeti E, Linē A, Lipps G, Llorente A, Lötvall J, Manček-Keber M, Marcilla A, Mittelbrunn M, Nazarenko I, Nolte-t Hoen EN, Nyman TA, O'Driscoll L, Olivan M, Oliveira C, Pállinger É, Del Portillo HA, Reventós J, Rigau M, Rohde E, Sammar M, Sánchez-Madrid F, Santarém N, Schallmoser K, Ostfeld MS, Stoorvogel W, Stukelj R, Van der Grein SG, Vasconcelos MH, Wauben MH and De Wever O. Biological properties of extracellular vesicles and their physiological functions. *J Extracell Vesicles* 2015; 4: 27066.
- [9] Li F, Wang Y, Lin L, Wang J, Xiao H, Li J, Peng X, Dai H and Li L. Mast cell-derived exosomes promote Th2 cell differentiation via OX40L-OX40 ligation. *J Immunol Res* 2016; 2016: 3623898.
- [10] Merluzzi S, Betto E, Ceccaroni AA, Magris R, Giunta M and Mion F. Mast cells, basophils and B cell connection network. *Mol Immunol* 2015; 63: 94-103.
- [11] Sangaphunchai P, Todd I and Fairclough LC. Extracellular vesicles and asthma: a review of the literature. *Clin Exp Allergy* 2020; 50: 291-307.
- [12] Yin Y, Shelke GV, Lasser C, Brismar H and Lötvall J. Extracellular vesicles from mast cells induce mesenchymal transition in airway epithelial cells. *Respir Res* 2020; 21: 101.
- [13] Pace E, Di Vincenzo S, Di Salvo E, Genovese S, Dino P, Sangiorgi C, Ferraro M and Gangemi S. MiR-21 upregulation increases IL-8 expression and tumorigenesis program in airway epithelial cells exposed to cigarette smoke. *J Cell Physiol* 2019; 234: 22183-22194.
- [14] Lee HY, Hur J, Kang JY, Rhee CK and Lee SY. MicroRNA-21 inhibition suppresses alveolar M2 macrophages in an ovalbumin-induced allergic asthma mice model. *Allergy Asthma Immunol Res* 2021; 13: 312-329.
- [15] Gras D, Chanez P, Vachier I, Petit A and Bourdin A. Bronchial epithelium as a target for innovative treatments in asthma. *Pharmacol Ther* 2013; 140: 290-305.
- [16] Liang Y, Huang S, Qiao L, Peng X, Li C, Lin K, Xie G, Li J, Lin L, Yin Y, Liao H, Li Q and Li L. Characterization of protein, long noncoding RNA and microRNA signatures in extracellular vesicles derived from resting and degranulated mast cells. *J Extracell Vesicles* 2020; 9: 1697583.
- [17] Elbehidy RM, Youssef DM, El-Shal AS, Shalaby SM, Sherbiny HS, Sherief LM and Akeel NE. MicroRNA-21 as a novel biomarker in diagnosis and response to therapy in asthmatic children. *Mol Immunol* 2016; 71: 107-114.
- [18] Kim RY, Horvat JC, Pinkerton JW, Starkey MR, Essilfie AT, Mayall JR, Nair PM, Hansbro NG, Jones B, Haw TJ, Sunkara KP, Nguyen TH, Jarnicki AG, Keely S, Mattes J, Adcock IM, Foster PS and Hansbro PM. MicroRNA-21 drives severe, steroid-insensitive experimental asthma by amplifying phosphoinositide 3-kinase-mediated suppression of histone deacetylase 2. *J Allergy Clin Immunol* 2017; 139: 519-532.
- [19] Sheedy FJ. Turning 21: induction of miR-21 as a key switch in the inflammatory response. *Front Immunol* 2015; 6: 19.
- [20] Liu MW, Liu R, Wu HY, Li YY, Su MX, Dong MN, Zhang W and Qian CY. Radix puerariae extracts ameliorate paraquat-induced pulmonary fibrosis by attenuating follistatin-like 1 and nuclear factor erythroid 2p45-related factor-2 signalling pathways through downregulation of miRNA-21 expression. *BMC Complement Altern Med* 2016; 16: 11.
- [21] Yang J, Kim EK, Park HJ, McDowell A and Kim YK. The impact of bacteria-derived ultrafine dust particles on pulmonary diseases. *Exp Mol Med* 2020; 52: 338-347.
- [22] Lee HY, Lee HY, Choi JY, Hur J, Kim IK, Kim YK, Kang JY and Lee SY. Inhibition of MicroRNA-21 by an antagomir ameliorates allergic inflammation in a mouse model of asthma. *Exp Lung Res* 2017; 43: 109-119.
- [23] Kuang DB, Zhou JP, Yu LY, Zeng WJ, Xiao J, Zhu GZ, Zhang ZL and Chen XP. DDAH1-V3 transcript might act as miR-21 sponge to maintain balance of DDAH1-V1 in cultured HUVECs. *Nitric Oxide* 2016; 60: 59-68.
- [24] Kinker KG, Gibson AM, Bass SA, Day BP, Deng J, Medvedovic M, Figueroa JA, Hershey GK and

## miR-21 derived from EVs promotes asthma

- Chen W. Overexpression of dimethylarginine dimethylaminohydrolase 1 attenuates airway inflammation in a mouse model of asthma. *PLoS One* 2014; 9: e85148.
- [25] Zhao C, Li T, Han B, Yue W, Shi L, Wang H, Guo Y and Lu Z. DDAH1 deficiency promotes intracellular oxidative stress and cell apoptosis via a miR-21-dependent pathway in mouse embryonic fibroblasts. *Free Radic Biol Med* 2016; 92: 50-60.
- [26] Liu XJ, Hong Q, Wang Z, Yu YY, Zou X and Xu LH. MicroRNA21 promotes interstitial fibrosis via targeting DDAH1: a potential role in renal fibrosis. *Mol Cell Biochem* 2016; 411: 181-189.

## Supplementary Materials

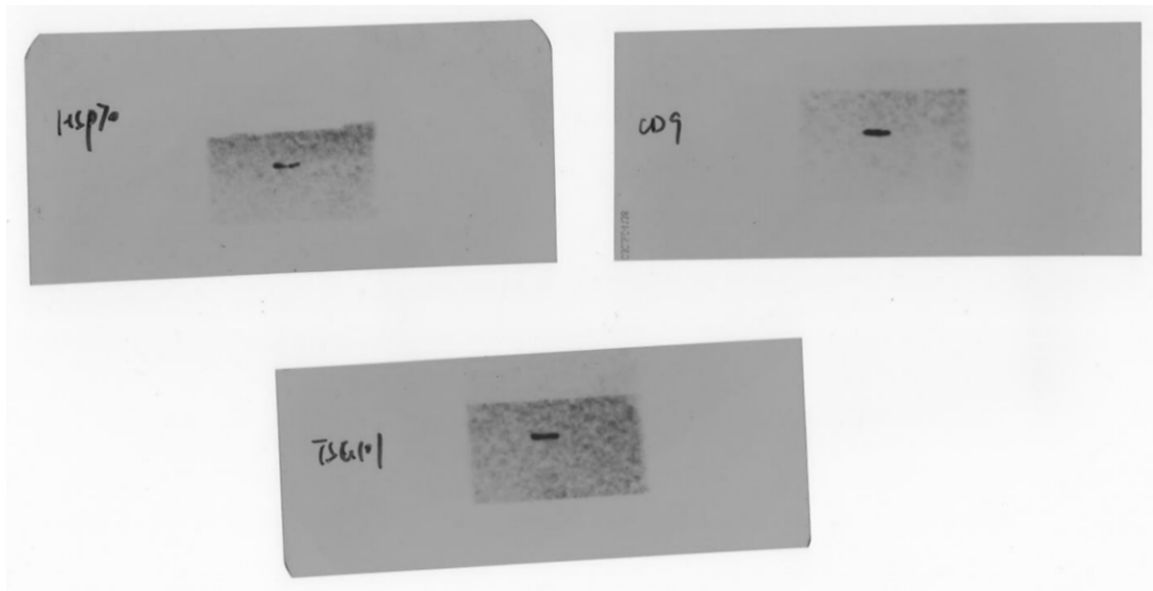


Figure S1. Western blots of Figure 2D.

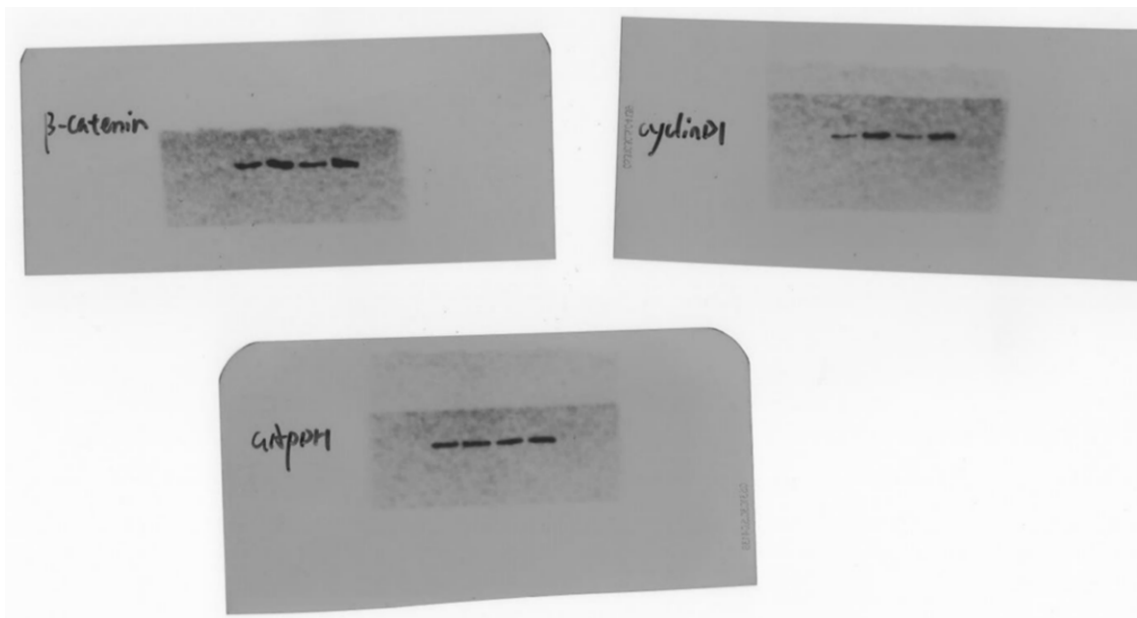


Figure S2. Western blots of Figure 6F.

miR-21 derived from EVs promotes asthma

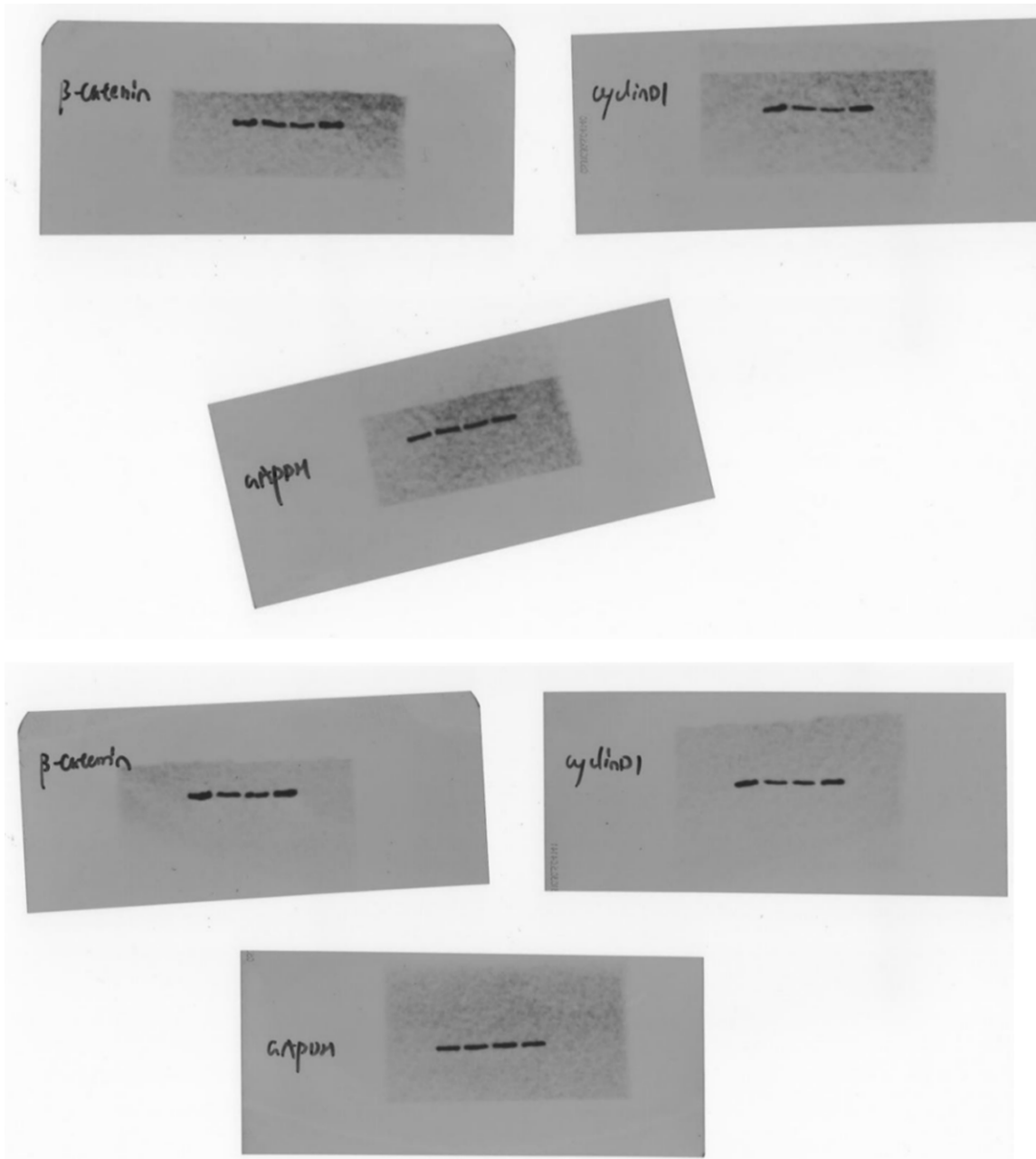


Figure S3. Western blots of Figure 6G.

miR-21 derived from EVs promotes asthma

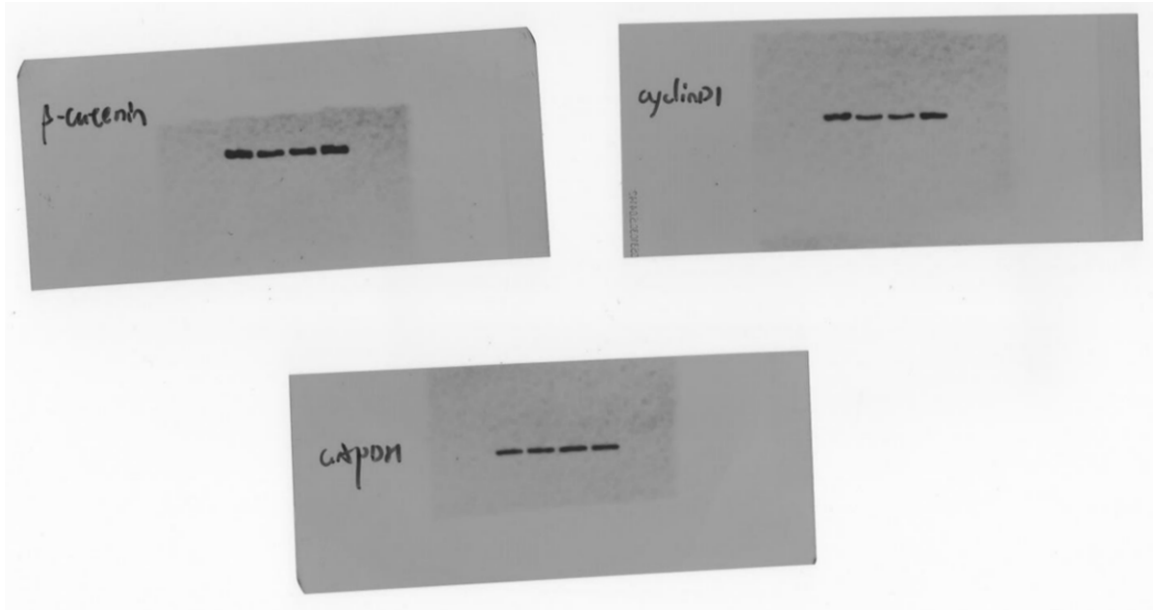


Figure S4. Western blots of Figure 6H.